

# A Preliminary Study on the Effects of Roll Dynamics in Predictive Vehicle Stability Control

G. Palmieri, P. Falcone, H. E. Tseng and L. Glielmo

**Abstract**—A Model Predictive Control (MPC) -based approach is presented for autonomous path following via Active Front Steering (AFS). We start from the Nonlinear MPC (NMPC) problem formulations in [2] and [4], where a simple bicycle model is used, and reformulate the same problem by using a more complex vehicle model including roll dynamics. We present and discuss simulation results of a vehicle autonomously performing high speed double lane change maneuvers, where load transfer effects due to roll dynamics become relevant. The results demonstrate that the inclusion of the roll dynamics in the prediction model of the MPC controller significantly improves the vehicle behavior at high speed on high friction surfaces, when significant lateral load transfers occur.

## I. INTRODUCTION

Over the past years, the cost reduction in sensors and computing systems, as well as the increasing demand of improved overall vehicle safety, encouraged a fast development and release of advanced active safety systems.

While the early vehicle dynamics control systems were primarily focused on improving the longitudinal and yaw motions by using differential braking and engine torque [4], recent advances in transmission and vehicle design can provide an increased number of possible interventions to influence the vehicle behavior. In particular, equipments such as Active Front Steering (AFS), Four Wheels Steering (4WS), active differentials [10] and active or semi-active suspensions can be integrated in existing or new active safety systems in order to improve the safety, the comfort and the agility of the vehicle. The problem of coordinating such large number of actuators in order to simultaneously control multiple vehicle dynamics is often referred to as Global Chassis Control (GCC) problem. Such design problem might be quite involving depending on the vehicle configuration (i.e., number of actuators) and the considered scenario (i.e., dynamics to be controlled, operating constraints).

In our recent works [2], [4], [7], [8], [3], [6], [5] we investigated Model Predictive Control (MPC) formulations solving such class of control problems. We have considered two autonomous path following scenarios where the vehicle has to be stabilized along the target path, at a given forward speed on slippery surfaces. In the two scenarios, simultaneous yaw and lateral stabilizations are accomplished

by controlling the front steering and coordinating the use of front steering and independent braking at the four wheels, respectively. In [2], [4], [7], [3] we presented MPC-based path following approaches where the control input is the front steering angle. In the MPC schemes presented in [8], [3], [6], instead, both front steering and the independent braking at the four wheels are used in order to best follow the desired path. We point out that we focused on traveling speed and road conditions such that the vehicle operates in regions of the state and input spaces where the plant nonlinearities (i.e., tire forces characteristics) become relevant.

In the scenarios considered in our previous works, however, load transfer effects can be neglected due to the considered low friction surfaces. In this paper, instead, we consider path following via AFS scenarios with friction surfaces ranging from snow to dry asphalt where lateral load transfer effects, due to roll motion, are significant.

In particular, we compare the autonomous path following controller in [2], [4] against an MPC controller based on a more complex vehicle model including the roll dynamics and accounting for the lateral load transfer. We compare the two approaches for different values of the road friction coefficient and the entry speed.

The paper is organized as follows. Section II presents the vehicle dynamical model. Section III formulates the path following via active front steering NMPC problem by using the vehicle model presented in Section II. In Section IV the simulation results are presented and discussed.

## II. MODELING

In this section we present the vehicle model, sketched in Figure 1, describing the motion of the vehicle in an inertial frame, subject to the lateral, longitudinal, yaw and roll dynamics. Figure 1(a) shows a top view of the vehicle in the inertial frame and explain the nomenclature related to the lateral, longitudinal and yaw dynamics. Figures 1(b) and 1(c) show front and lateral views of the vehicle, respectively, explaining the nomenclature related to the roll dynamics.

The model is presented in [11] and reported next for the sake of completeness. We use two subscript symbols to denote variables related to the four wheels. In particular  $\star \in \{f, r\}$  denotes the front and rear axles, while  $\bullet \in \{l, r\}$  denotes the left and right sides of the vehicle. As example, the variable  $(\cdot)_{f,l}$  is referred to the front left wheel. Moreover we use the following nomenclature.

G. Palmieri and L. Glielmo are with Dipartimento di Ingegneria Università del Sannio, 82100 Benevento, Italy. E-mail: {giovanni.palmieri, glielmo}@unisannio.it

P. Falcone is with Department of Signals and Systems, Chalmers University of Technology, SE-412 96 Göteborg, Sweden, E-mail: falcone@chalmers.se

H. E. Tseng is with the Ford Research Laboratories Dearborn, MI 48124, USA. E-mail: htseng@ford.com

$$m_t(\ddot{y} + \dot{\psi}\dot{x}) = F_{y_{f,l}} + F_{y_{f,r}} + F_{y_{r,l}} + F_{y_{r,r}} + (b-a)m_u\ddot{\psi} + h_{rc}m_s\ddot{\phi}, \quad (1)$$

$$m_t(\ddot{x} - \dot{\psi}\dot{y}) = F_{x_{f,l}} + F_{x_{f,r}} + F_{x_{r,l}} + F_{x_{r,r}} + (a-b)m_u\dot{\psi}^2 - 2h_{rc}m_s\dot{\psi}\dot{\phi}, \quad (2)$$

$$I_z\ddot{\psi} + I_{xz}\ddot{\phi} = a(F_{y_{f,l}} + F_{y_{f,r}}) - b(F_{y_{r,l}} + F_{y_{r,r}}) + c(-F_{x_{f,l}} + F_{x_{f,r}} - F_{x_{r,l}} + F_{x_{r,r}}) + (b-a)m_u(\ddot{y} + \dot{\psi}\dot{x}), \quad (3)$$

$$(I_x + m_s h_{rc}^2)\ddot{\phi} + I_{xz}\ddot{\psi} = m_s g h_{rc} \phi - 2k_\phi \phi - 2b_\phi \dot{\phi} + m_s h_{rc} (\ddot{y} + \dot{\psi}\dot{x}), \quad (4)$$

**NOMENCLATURE:**

|                          |  |
|--------------------------|--|
| $a$                      | distance of CoG from front axle [m]  |
| $b$                      | distance of CoG from rear axle [m]   |
| $c$                      | half track width [m]   |
| $h_{CoG}$                | CoG height [m]   |
| $h_{rcf}$                | front roll center distance below sprung mass CoG [m]                                   |
| $h_{rcr}$                | rear roll center distance below sprung mass CoG [m]                                    |
| $I_{xx}$                 | momentum of inertia around the roll axis [kgm <sup>2</sup> ]                           |
| $I_{xz}$                 | product of inertia [kgm <sup>2</sup> ]   |
| $I_{zz}$                 | momentum of inertia around the $z$ -axis [kgm <sup>2</sup> ]                           |
| $I_w$                    | wheel and driveline inertia [kgm <sup>2</sup> ]  |
| $m_s$                    | vehicle sprung mass [kg]   |
| $m_u$                    | vehicle un-sprung mass [kg]  |
| $m_t$                    | total vehicle mass [kg]  |
| $\dot{x}, \dot{y}$       | longitudinal, lateral velocities of CoG in the body frame [m/s]                        |
| $X, Y$                   | car position in the inertial frame [m]   |
| $\phi$                   | roll angle [rad]   |
| $\psi$                   | yaw angle [rad]  |
| $\dot{\phi}, \dot{\psi}$ | roll rate, yaw rate [rad/s]  |
| $b_\phi$                 | equivalent suspension damping coefficient [N · m · s]                                  |
| $k_\phi$                 | equivalent suspension roll stiffness [N · m]   |
| $F_l, F_c, F_z$          | longitudinal, lateral, normal tire forces [N]  |
| $F_y, F_x$               | tire forces components along lateral and longitudinal axes in the body frame [N]       |
| $r_w$                    | tire nominal radius [m]  |
| $v_c, v_l$               | lateral and longitudinal tire velocities [m/s]   |
| $v_x, v_y$               | tire velocities components along lateral and longitudinal axes in the body frame [m/s] |
| $\omega$                 | wheel angular speed [rad/s]  |
| $b_w$                    | wheel and driveline damping coefficient [Nm s]   |
| $\alpha$                 | tire slip angle [rad]  |
| $s$                      | tire slip ratio [%]  |
| $\delta_f$               | front steering angle [rad]   |
| $T_b$                    | braking torques at the braking pads [Nm]   |

The lateral, longitudinal, yaw and roll vehicle motions are described through the nonlinear differential equations (1)-(4), where the components  $F_{y_{*,\bullet}}$  and  $F_{x_{*,\bullet}}$  of the tire forces, along the lateral and longitudinal vehicle axes, respectively,

are computed as follows

$$F_{y_{*,\bullet}} = F_{l_{*,\bullet}} \sin \delta_* + F_{c_{*,\bullet}} \cos \delta_*, \quad (5a)$$

$$F_{x_{*,\bullet}} = F_{l_{*,\bullet}} \cos \delta_* - F_{c_{*,\bullet}} \sin \delta_*. \quad (5b)$$

The lateral and longitudinal tire forces  $F_{c_{*,\bullet}}$  and  $F_{l_{*,\bullet}}$  are computed as

$$F_{c_{*,\bullet}} = f_c(\alpha_{*,\bullet}, s_{*,\bullet}, \mu_{*,\bullet}, F_{z_{*,\bullet}}), \quad (6a)$$

$$F_{l_{*,\bullet}} = f_l(\alpha_{*,\bullet}, s_{*,\bullet}, \mu_{*,\bullet}, F_{z_{*,\bullet}}). \quad (6b)$$

The lateral and longitudinal tire characteristics  $f_c$  and  $f_l$  are based on the Pacejka tire model [1], [4], [2]. This is a static nonlinear tire model computing the tire forces in combined braking/driving and cornering manoeuvres.

The slip angle  $\alpha_{*,\bullet}$  in (6) represents the angle between the wheel velocity vector  $v_{*,\bullet}$  and the direction of the wheel itself, and can be compactly expressed as:

$$\alpha_{*,\bullet} = \arctan \frac{v_{c_{*,\bullet}}}{v_{l_{*,\bullet}}}. \quad (7)$$

The wheel's equations of motion describe the lateral (or cornering) and longitudinal wheel velocities:

$$v_{c_{*,\bullet}} = v_{y_{*,\bullet}} \cos \delta_* - v_{x_{*,\bullet}} \sin \delta_*, \quad (8a)$$

$$v_{l_{*,\bullet}} = v_{y_{*,\bullet}} \sin \delta_* + v_{x_{*,\bullet}} \cos \delta_*, \quad (8b)$$

where the velocities  $v_{x_{*,\bullet}}$  and  $v_{y_{*,\bullet}}$  for the four wheels are computed as follows:

$$v_{y_{f,l}} = \dot{y} + a\dot{\psi} \quad v_{x_{f,l}} = \dot{x} - c\dot{\psi}, \quad (9a)$$

$$v_{y_{f,r}} = \dot{y} + a\dot{\psi} \quad v_{x_{f,r}} = \dot{x} + c\dot{\psi}, \quad (9b)$$

$$v_{y_{r,l}} = \dot{y} - b\dot{\psi} \quad v_{x_{r,l}} = \dot{x} - c\dot{\psi}, \quad (9c)$$

$$v_{y_{r,r}} = \dot{y} - b\dot{\psi} \quad v_{x_{r,r}} = \dot{x} + c\dot{\psi}. \quad (9d)$$

The slip ratios  $s_{*,\bullet}$  in (6) are defined as

$$s_{*,\bullet} = \begin{cases} \frac{r_w \omega_{*,\bullet}}{v_{l_{*,\bullet}}} - 1 & \text{if } v_{l_{*,\bullet}} > r_w \omega_{*,\bullet}, v_{l_{*,\bullet}} \neq 0 \text{ for braking} \\ 1 - \frac{v_{l_{*,\bullet}}}{r_w \omega_{*,\bullet}} & \text{if } v_{l_{*,\bullet}} < r_w \omega_{*,\bullet}, \omega_{*,\bullet} \neq 0 \text{ for driving.} \end{cases} \quad (10)$$

The wheel angular speeds  $\omega_{*,\bullet}$  in (10) are obtained by integrating the following set of differential equations:

$$I_{w_{*,\bullet}} \dot{\omega}_{*,\bullet} = -F_{l_{*,\bullet}} r_w - T_{b_{*,\bullet}} - b_w \cdot \omega_{*,\bullet}. \quad (11)$$

The tire normal forces  $F_{z_{*,\bullet}}$  in (6) are computed as in equations (12)-(15), where

$$F_{z_f,l} = \frac{1}{2} \left( \frac{bmg}{(a+b)} - F_{y_f} \phi \right) - \frac{k_{\phi_f} \phi}{2c} - \frac{b_{\phi_f} \dot{\phi}}{2c} - \frac{h_{rc_f}}{2c} \left( F_{y_f} + \frac{bmg}{(a+b)} \phi \right), \quad (12)$$

$$F_{z_f,r} = \frac{1}{2} \left( \frac{bmg}{(a+b)} - F_{y_f} \phi \right) + \frac{k_{\phi_f} \phi}{2c} + \frac{b_{\phi_f} \dot{\phi}}{2c} + \frac{h_{rc_f}}{2c} \left( F_{y_f} + \frac{bmg}{(a+b)} \phi \right), \quad (13)$$

$$F_{z_r,l} = \frac{1}{2} \left( \frac{amg}{(a+b)} - F_{y_r} \phi \right) - \frac{k_{\phi_r} \phi}{2c} - \frac{b_{\phi_r} \dot{\phi}}{2c} - \frac{h_{rc_r}}{2c} \left( F_{y_r} + \frac{amg}{(a+b)} \phi \right), \quad (14)$$

$$F_{z_r,r} = \frac{1}{2} \left( \frac{amg}{(a+b)} - F_{y_r} \phi \right) + \frac{k_{\phi_r} \phi}{2c} + \frac{b_{\phi_r} \dot{\phi}}{2c} + \frac{h_{rc_r}}{2c} \left( F_{y_r} + \frac{amg}{(a+b)} \phi \right), \quad (15)$$

$$F_{y_f} = F_{y_f,l} + F_{y_f,r}, \quad (16a)$$

$$F_{y_r} = F_{y_r,l} + F_{y_r,r}. \quad (16b)$$

We point out that in the normal tire forces (12)-(15) (i) only the effects of the lateral load transfers are included, i.e., load transfers due to longitudinal accelerations are not modeled and (ii) small angle approximations are used for  $\cos \phi$  and  $\sin \phi$ .

Finally the motion of the vehicle in the inertial frame  $X$ - $Y$  is described by the following two differential equations

$$\dot{Y} = \dot{x} \sin \psi + \dot{y} \cos \psi, \quad (17a)$$

$$\dot{X} = \dot{x} \cos \psi - \dot{y} \sin \psi. \quad (17b)$$

Using the equations (1)-(17) the nonlinear vehicle dynamics can be described by the following compact differential equation:

$$\dot{\xi}(t) = f_{\mu(t)}(\xi(t), u(t)), \quad (18)$$

where the state and input vectors are  $\xi = [\dot{y}, \dot{x}, \psi, \dot{\psi}, \phi, \dot{\phi}, Y, X, \omega_{f,l}, \omega_{f,r}, \omega_{r,l}, \omega_{r,r}]$  and  $u = [\delta_f, T_{b_f,l}, T_{b_f,r}, T_{b_r,l}, T_{b_r,r}]$ , respectively, and  $\mu(t) = [\mu_{f,l}(t), \mu_{f,r}(t), \mu_{r,l}(t), \mu_{r,r}(t)]$ .

### III. MPC PROBLEM FORMULATION

In this section we formulate the considered path following problem as a Model Predictive Control problem as in [4], [2], [3].

*Assumption 1:* Next we assume  $T_{b_{*,\bullet}} = 0$  and  $\mu_{*,\bullet} = \hat{\mu}$ , with  $\hat{\mu}$  known, in (18), i.e., no braking and the same friction coefficient for the four wheels.

Under the Assumption 1, we discretize the system dynamics (18) with a fixed sampling time  $T_s$ :

$$\xi(t+1) = f_{\hat{\mu}(t)}^{dt}(\xi(t), u(t)), \quad (19a)$$

$$u(t) = u(t-1) + \Delta u(t), \quad (19b)$$

where the  $\Delta u$  formulation is used and  $u(t) = \delta_f(t)$ ,  $\Delta u(t) = \Delta \delta_f(t)$ .

We define the following output map for yaw angle, yaw rate and lateral position states:

$$\eta(t) = h(\xi(t)), \quad (20)$$

where  $\eta = [\psi, \dot{\psi}, Y]$ , and consider the following cost function:

$$J(\xi(t), \Delta \mathcal{U}_t) = \sum_{i=1}^{H_p} \left\| \eta_{t+i,t} - \eta_{ref_{t+i,t}} \right\|_Q^2 + \sum_{i=0}^{H_c-1} \left\| \Delta u_{t+i,t} \right\|_R^2 + \sum_{i=0}^{H_c-1} \left\| u_{t+i,t} \right\|_S^2, \quad (21)$$

where  $\Delta U(t) = [\Delta u(t), \dots, \Delta u(t+H_c-1)]$  is the optimization vector at time  $t$ ,  $\eta(t+i)$  denotes the output vector predicted at time  $t+i$  obtained by starting from the state  $\xi(t)$  and applying to system (19)-(20) the input sequence  $\Delta u(t), \dots, \Delta u(t+i)$ .  $\eta_{ref}$  is the output reference signal and  $H_p$  and  $H_c$  denote the output prediction horizon and the control horizon, respectively. In (21) the first summand reflects the penalty on trajectory tracking error while the second and third summands penalize the steering effort.  $Q$ ,  $R$  and  $S$  are weighting matrices of appropriate dimensions.

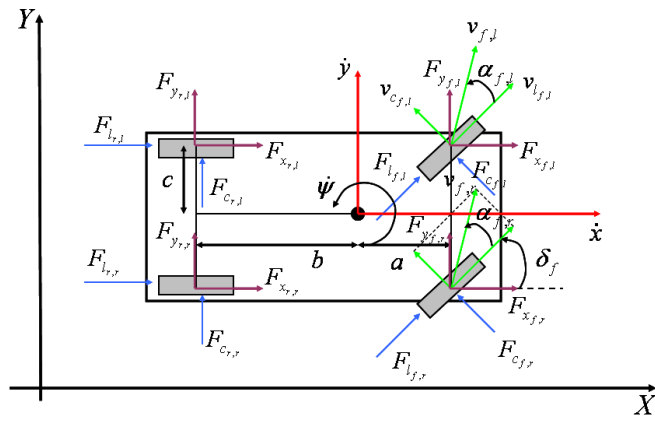
An optimization problem, based on the discrete time vehicle model (19)-(20) and the cost function (21), is formulated and solved in receding horizon as in [2], [4] to obtain the following state feedback control law

$$u(t, \xi(t)) = u(t-1) + \Delta u_{t,t}^*(t, \xi(t)), \quad (22)$$

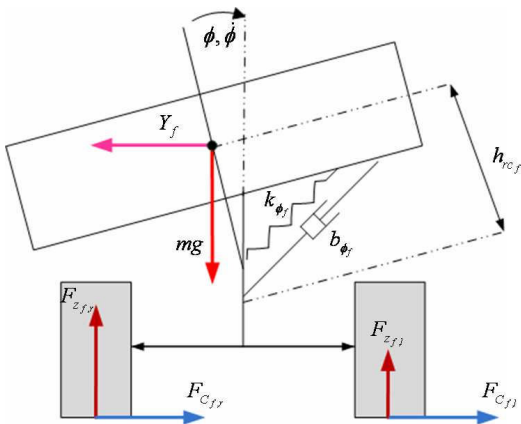
where  $u_{t,t}^*(t, \xi(t))$  is obtained as solution of the optimization problem.

### IV. SIMULATION RESULTS

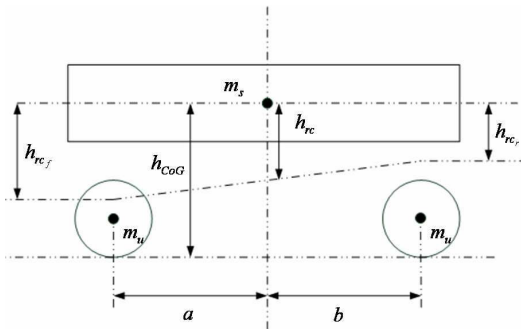
Next we present and discuss the simulation results of the path following algorithm presented in Section III, implemented to perform a double lane change manoeuvre. This test represents an obstacle avoidance emergency maneuver in which the vehicle is entering a double lane change with a given initial forward speed. The control input is the front steering angle and the goal is to follow the trajectory as close as possible by minimizing the vehicle deviation from the target path. The controller presented in Section III, next referred to as Controller A, is compared against a simpler MPC controller, next referred to as Controller B, derived from Controller A by neglecting the roll dynamics. We point out that (i) the only difference between Controller A and



TOP VIEW  
(a) Vehicle model. Top view.



FRONT VIEW  
(b) Vehicle model. Front view.



LATERAL VIEW  
(c) Vehicle model. Lateral view.

Fig. 1: Twelfth order states vehicle model.

Controller B is the vehicle model used in the problem formulation, i.e., instead of the twelfth order nonlinear model (18) a simpler tenth order nonlinear model is used in Controller B and (ii) in both controllers the control input is the front steering angle. Controller A and Controller B have been compared in a simulation scenario where the vehicle enters the double lane change at forward speeds, ranging from 50 to 130 Kph, on different road conditions, ranging from snow ( $\mu = 0.3$ ) to dry asphalt ( $\mu = 0.9$ ). For both controllers,

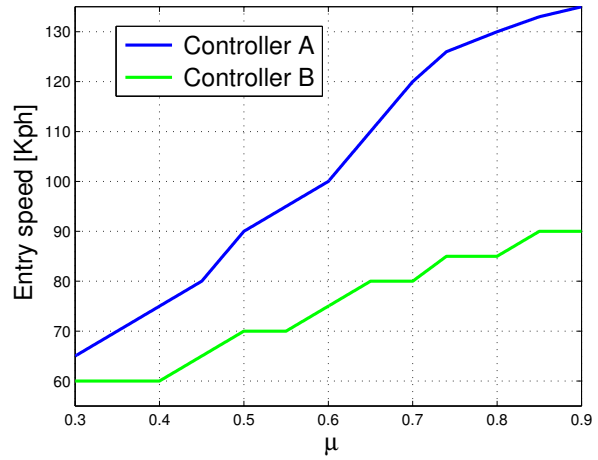


Fig. 2: Maximum entry speed for different road surfaces for the two controllers.

simulations have been performed in order to (i) estimate, for each considered road surface, the maximum entry speed the vehicle can perform the manoeuvre without losing the control and (ii) evaluate the tracking performances at different entry speeds on the considered road surfaces.

Controller A and Controller B have been implemented with the following parameters:

- sampling time:  $T = 0.05s$ .
- horizons:  $H_p = 15$ ,  $H_u = 1$ .
- bounds:
  - $\delta_{f,min} = -10$  deg,  $\delta_{f,max} = 10$  deg,  $\Delta\delta_{f,min} = -0.85$  deg,  $\Delta\delta_{f,max} = 0.85$  deg.
- weighting matrices:
  - $Q \in \mathbb{R}^{3 \times 3}$  with  $Q_{11} = 1$ ,  $Q_{22} = 1$ ,  $Q_{33} = 20$  and  $Q_{ij} = 0$  for  $i \neq j$ .
  - $R = 1$ .
  - $S = 5$ .

The commercial NPSOL software package [9] is used for implementing the MPC controllers in a Matlab environment.

*Remark 1:* In order to easily compare Controller A and Controller B, the same tuning parameters have been chosen for both controllers. In particular the above parameters have been selected by tuning Controller B in order to stabilize the vehicle along the path at the considered entry speeds.

In Figure 2 the maximum entry speed against the road friction coefficient is plotted for Controller A and Controller B. Not surprisingly, for both controllers, the maximum entry speed monotonically increases as the road friction coefficient  $\mu$  increases. We also observe that (i) as the road friction coefficient increases, the rise of the maximum entry speed is larger for Controller A than Controller B and (ii) on slippery surfaces ( $\mu = 0.3$ ) the maximum entry speeds for the two controllers are similar. In order to explain the behavior observed for the two controllers, we recall that Controller A includes vehicle roll dynamics while Controller B does not. The inclusion of roll dynamics in the prediction model significantly improves the performance of Controller A at

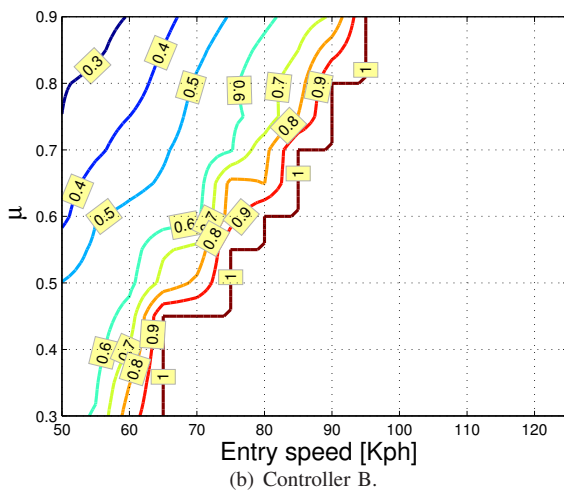
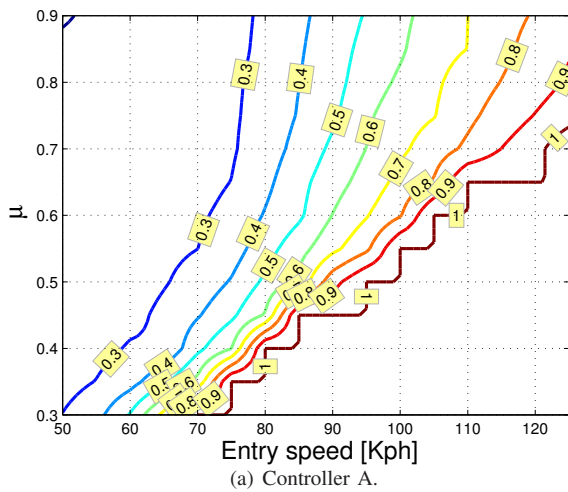


Fig. 3: Normalized lateral position RMS tracking error against road friction coefficient  $\mu$  and entry speed.

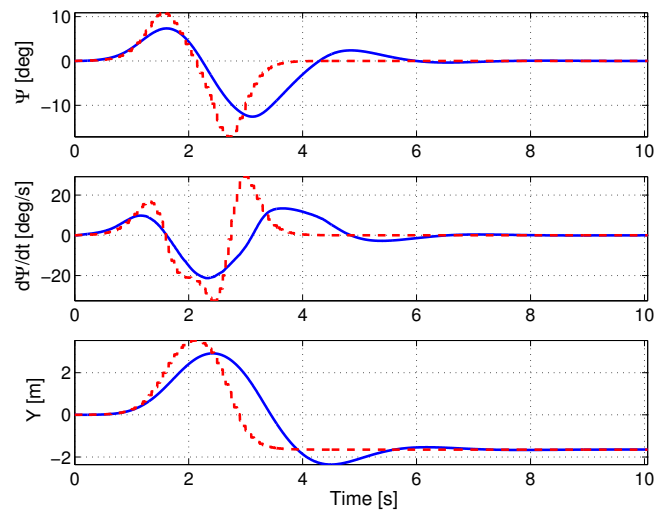
high speed on high- $\mu$  surfaces when roll dynamics become relevant. At low speed on low- $\mu$  surfaces, the maximum entry speed improvement in Controller A compared to Controller B is small since roll dynamics are negligible in the considered operating conditions.

*Remark 2:* We remark that in both Controller A and Controller B, instability can occur at high entry speed since a finite time horizon optimal control problem is solved each time step.

In Figure 3, lateral position Root Mean Squared (RMS) tracking errors for Controller A (Figure 3(a)) and Controller B (Figure 3(b)) are reported. For each controller, isolines of the RMS errors are plotted against the vehicle entry speed and the road friction coefficient. In order to compute the RMS tracking errors, the following formula is used

$$Y_{rms}(\bar{x}, \mu) = \sqrt{\frac{1}{X_{end}} \sum_{i=1}^{i=N} [Y(X_i, \bar{x}, \mu) - Y_{ref}(X_i)]^2}, \quad (23)$$

where  $\bar{x}$  is the forward entry speed,  $Y(\cdot, \cdot, \cdot)$  is the vehicle



(a) Controller A. Tracking variables. Yaw angle (upper plot), yaw rate (middle plot) and lateral position (lower plot). Solid and dashed lines are the actual and reference signals, respectively.

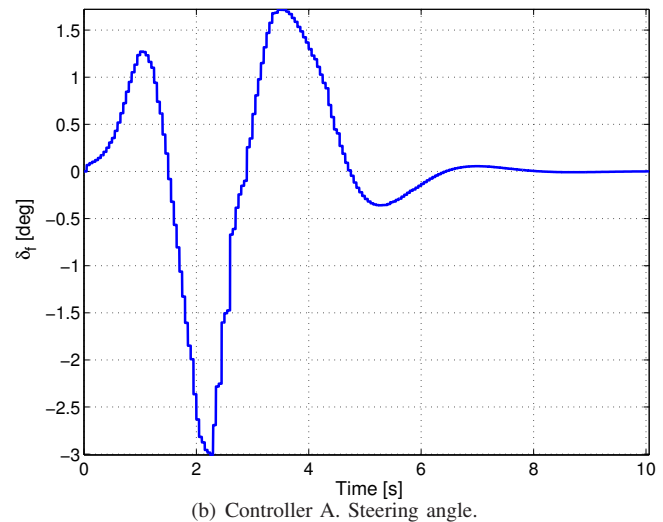
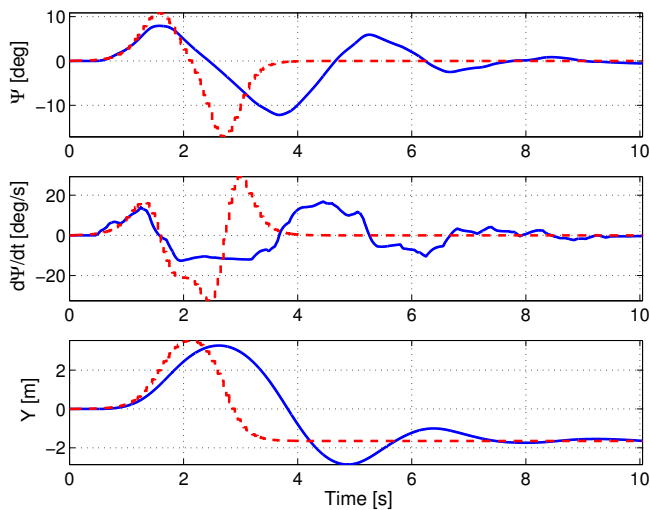


Fig. 4: Controller A. Double lane change manoeuvre at 90 Kph on dry asphalt ( $\mu = 0.9$ ).

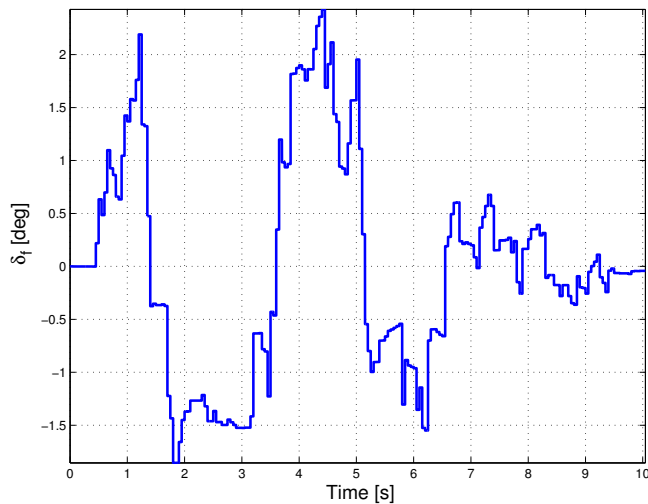
lateral position in the inertial frame,  $Y_{ref}(\cdot)$  is the target path and  $X_{end}$  is the longitudinal coordinate of the manoeuvre ending point. We remark that the target path does not depend on the friction coefficient and the forward entry speed.

Not surprisingly the performances of Controller B are worse than Controller A, hence, in order to easily compare the two controllers, the RMS data have been normalized to the maximum tracking error of Controller B. Moreover, such value is used to mark the operating conditions (i.e., entry speed and road surface) at which the vehicle is unstable. The regions delimited by the isolines labeled with ‘1’ denote such operating conditions. For instance, when the vehicle with Controller A enters the double lane change at 120 Kph on a sandy surface ( $\mu = 0.5$ ) is unstable.

By comparing the RMS errors of Controller A and Controller B we observe that the operating region where Controller B is unstable is wider than Controller A. Moreover,



(a) Controller B. Tracking variables. Yaw angle (upper plot), yaw rate (middle plot) and lateral position (lower plot). Solid and dashed lines are the actual and reference signals, respectively.



(b) Controller B. Steering angle.

Fig. 5: Controller B. Double lane change manoeuvre at 90 Kph on dry asphalt ( $\mu = 0.9$ ).

the RMS error isolines of Controller B show significant performance degradation, compared to Controller A, on high- $\mu$  surfaces. On the other hand, the performances of the two controllers at low entry speed on low- $\mu$  surfaces are closer and confirm the trend observed in Figure 2 for the maximum entry speeds.

Finally, simulation results of a double lane change manoeuvre at 90 Kph on dry asphalt ( $\mu = 0.9$ ) for Controller A and Controller B are reported in Figures 4 and 5, respectively. We observe that yaw rate in Controller B saturates at  $-10$  deg between 2 and almost 3.5 s, while in the same time interval, Controller A performs a more aggressive manoeuvres (yaw rate is up to  $-20$  deg) and significantly improves the path following. We also observe that steering angle in Controller A is much smoother than Controller B.

## V. CONCLUSIONS

We presented a performance analysis of a path following Nonlinear Model Predictive Control approach via active front steering. In particular we evaluated the impact of the lateral load transfer due to the roll dynamics on stability limits and performance of the controller in [2] when double lane changes are performed at different entry speeds on different surfaces. The results confirm that the inclusion of roll dynamics in the vehicle prediction model significantly improves the performance of the approach on high speed and high- $\mu$  surfaces. The obtained results represent a further step toward the design of predictive GCC approaches including, for instance, roll-over prevention/avoidance functionalities.

## REFERENCES

- [1] E. Bakker, L. Nyborg, and H. B. Pacejka. Tyre modeling for use in vehicle dynamics studies. *SAE paper # 870421*, 1987.
- [2] F. Borrelli, P. Falcone, T. Keviczky, J. Asgari, and D. Hrovat. MPC-based approach to active steering for autonomous vehicle systems. *Int. J. Vehicle Autonomous Systems*, 3(2/3/4):265–291, 2005.
- [3] P. Falcone. *Nonlinear Model Predictive Control for Autonomous Vehicles*. PhD thesis, Università del Sannio, Dipartimento di Ingegneria, Piazza Roma 21, 82100, Benevento, Italy, June 2007.
- [4] P. Falcone, F. Borrelli, J. Asgari, H. E. Tseng, and D. Hrovat. Predictive active steering control for autonomous vehicle systems. *IEEE Trans. on Control System Technology*, 15(3), 2007.
- [5] P. Falcone, F. Borrelli, J. Asgari, H. E. Tseng, and D. Hrovat. Linear time varying model predictive control and its application to active steering systems: Stability analysis and experimental validation. *International Journal of Robust and Nonlinear Control*, 18:862–875, 2008.
- [6] P. Falcone, F. Borrelli, J. Asgari, H. E. Tseng, and D. Hrovat. Mpc-based yaw and lateral stabilization via active front steering and braking. *Vehicle System Dynamics*, 46, Supplement:611–628, 2008.
- [7] P. Falcone, F. Borrelli, J. Asgari, H. Eric Tseng, and D. Hrovat. A real-time model predictive control approach for autonomous active steering. In *Nonlinear Model Predictive Control for Fast Systems, Grenoble, France*, 2006.
- [8] P. Falcone, F. Borrelli, H. E. Tseng, J. Asgari, and D. Hrovat. Integrated braking and steering model predictive control approach in autonomous vehicles. *Fift IFAC Symposium on Advances of Automotive Control*, 2007.
- [9] P. Gill, W. Murray, M. Saunders, and M. Wright. NPSOL – Nonlinear Programming Software. Stanford Business Software, Inc., Mountain View, CA, 1998.
- [10] D. Piyabongkarn, R. Rajamani, J. Y. Lew, and H. Yu. On the use of torque-biasing devices for vehicle stability control. 2006.
- [11] T. Shim and C. Ghike. Understanding the limitations of different vehicle models for roll dynamics studies. *Vehicle System Dynamics*, 45:191–216, March 2007.